GLIA

WILEY

Differential interaction with TREM2 modulates microglial uptake of modified Aβ species

Pranav Joshi[1] | Florian Riffel[1] | Kanayo Satoh[2] | Masahiro Enomoto[3] | Seema Qamar[4] | Hannah Scheiblich[5,6] | Nàdia Villacampa[5,6] | Sathish Kumar[1] | Sandra Theil[1] | Samira Parhizkar[7] | Christian Haass[7,8,9] | Michael T. Heneka[5,6] | Paul E. Fraser[2] | Peter St George-Hyslop[2,4] | Jochen Walter[1]

[1]Department of Neurology, University of Bonn, Bonn, Germany

[2]Departments of Medical Biophysics and Medicine (Neurology), Tanz Centre for Research in Neurodegenerative Diseases and, Toronto, Ontario, Canada

[3]Princess Margaret Cancer Centre Research Institute, University Health Network, Toronto, Ontario, Canada

[4]Cambridge Institute for Medical Research, Department of Clinical Neurosciences, School of Clinical Medicine, University of Cambridge, Cambridge, UK

[5]Department of Neurodegenerative Diseases and Gerontopsychiatry, University Hospital Bonn, Bonn, Germany

[6]Neuroinflammation Unit, German Center for Neurodegenerative Diseases e. V. (DZNE), Bonn, Germany

[7]Chair of Metabolic Biochemistry, Biomedical Center (BMC), Faculty of Medicine, Ludwig-Maximilians-Universität München, Munich, Germany

[8]Munich Cluster for Systems Neurology (SyNergy), Munich, Germany

[9]Molecular Neurodegeneration Unit, German Center for Neurodegenerative Diseases e.V. (DZNE) Munich, Munich, Germany

Correspondence
Jochen Walter, Department of Neurology, University of Bonn, Venusberg-Campus 1, (Formerly Sigmund-Freud-Str. 25), 53127 Bonn, Germany.
Email: jochen.walter@ukbonn.de

Abstract

Rare coding variants of the microglial triggering receptor expressed on myeloid cells 2 (TREM2) confer an increased risk for Alzheimer's disease (AD) characterized by the progressive accumulation of aggregated forms of amyloid β peptides (Aβ). Aβ peptides are generated by proteolytic processing of the amyloid precursor protein (APP). Heterogeneity in proteolytic cleavages and additional post-translational modifications result in the production of several distinct Aβ variants that could differ in their aggregation behavior and toxic properties. Here, we sought to assess whether post-translational modifications of Aβ affect the interaction with TREM2. Biophysical and biochemical methods revealed that TREM2 preferentially interacts with oligomeric Aβ, and that phosphorylation of Aβ increases this interaction. Phosphorylation of Aβ also affected the TREM2 dependent interaction and phagocytosis by primary microglia and in APP transgenic mouse models. Thus, TREM2 function is important for sensing phosphorylated Aβ variants in distinct aggregation states and reduces the accumulation and deposition of these toxic Aβ species in preclinical models of Alzheimer's disease.

KEYWORDS
Alzheimer's disease, amyloid β, FTD mutation, phosphorylation, post-translational modification, TREM2

1 | INTRODUCTION

Progressive accumulation of amyloid-β (Aβ) in form of extracellular plaques along with intracellular deposition of hyperphosphorylated tau protein in neurofibrillary tangles (NFT) are classical pathological hallmarks of Alzheimer's disease (AD) (d'Errico & Meyer-Luehmann, 2020; Haass & Selkoe, 2007; Hyman et al., 2012; Selkoe & Hardy, 2016). Aβ deposits can also be detected intracellularly, particularly inside of neurons (Gouras et al., 2010; Gouras et al., 2012; Kumar et al., 2013; Wirths et al., 2009) and within the vasculature of the brain (Huang et al., 2021; Spangenberg et al., 2019; Thal et al., 2008; Thal et al., 2009). Aβ peptides can undergo post-translational modifications that alter aggregation and neurotoxic characteristics and might thereby modulate the pathogenesis of AD (Barykin et al., 2017; Kummer & Heneka, 2014). For example, N-terminal truncation and formation of pyroglutamate at position 3 of the Aβ peptide strongly promotes aggregation, and pyroglutamate modified Aβ species are abundant in AD brain (Saido et al., 1995; Schilling et al., 2008). Phosphorylation of Aβ at serine 8 also promotes aggregation into oligomeric and fibrillar assemblies (Kumar et al., 2011), while phosphorylation at serine 26 leads to formation of stable neurotoxic oligomers (Kumar et al., 2016).

During disease progression, brain-resident microglia cluster around extracellular Aβ plaques to prevent further growth or deposition thereby limiting neuritic dystrophy (Condello et al., 2015). Microglia depletion also altered parenchymal plaque development and promoted Aβ deposition in cortical blood vessels (Spangenberg et al., 2019).

Recent studies identified sequence variants in the triggering receptor expressed on myeloid cells 2 (TREM2) that are associated with an increased risk for several neurodegenerative disorders such as AD (Guerreiro, A. Wojtas, et al., 2013; Jonsson et al., 2013). TREM2 binds anionic ligands, including certain phospholipids and apolipoproteins (Bailey et al., 2015; Kober & Brett, 2017; Yeh et al., 2016). In addition, TREM2 has also been shown to bind Aβ, and affect its clearance and aggregation (Kober et al., 2020; Lessard et al., 2018; Vilalta et al., 2021; Zhao et al., 2018; Zhong et al., 2018). However, little is known about how post-translationally modified Aβ variants in various aggregation states are handled by microglia and whether this is TREM2 dependent.

In this study, we demonstrate that posttranslational modifications of Aβ differentially affect the binding to TREM2. Furthermore, we report that TREM2 is involved in the differential internalization of modified Aβ variants by microglia, and the characteristic deposition in brains of transgenic mouse models of AD.

2 | METHODS

2.1 | Processing of Aβ peptides

The synthetic Aβ(1–42) and Aβ(3–42) peptide variants were obtained from PSL, GmbH. Synthetic Biotin-LC-Aβ(1–42) (LC: 6-carbon long chain) was obtained from AnaSpec. The synthetic Aβ peptides used in this study showed greater than 95% purity by HPLC (data available on request). The reconstitution of Aβ peptide variants was done by adding 10 mM NaOH directly to the vial to make a stock solution of 230 μM followed by sonication for 5 min, aliquoted and snap-frozen. Biotin-LC-Aβ(1–42) was reconstituted with DMSO and biolayer interferometry (BLI) assay buffer (consisting of 20 mM HEPES and 1 M NaCl) thus giving a stock concentration of 100 μM, aliquoted and snap-frozen.

For the preparation of Aβ oligomers we used two different methods:

2.1.1 | Method 1

For the dot blot, and BLI experiments, we used oAβ(1–42) preparation made by gently mixing freshly prepared Aβ(1–42) variants separately with a suitable concentration of Biotin-LC-Aβ(1–42) to make the final concentration of 23 μM in PBS (pH 7.4) followed by incubation at 37°C for 3 h (Vilalta et al., 2021).

2.1.2 | Method 2

For the pulldown, and cellular binding and phagocytosis experiments, we followed protocol to prepare oAβ as described previously (T. Kim et al., 2013). Briefly, monomeric Aβ stock was diluted to 100 μM in PBS and incubated at 23°C for 16 h followed by an incubation at 4°C for 24 h. The preparation was further centrifuged at 16,000*g* and the supernatant aliquoted, flash frozen in liquid nitrogen and stored at −20°C.

2.2 | Transmission electron microscopy

oAβ prepared using method 1 were characterized by negative stain-transmission electron microscopy (TEM) as described by Anderson et al. (2010). Briefly, 5–10 μl of oAβ at a concentration of 1 μM were placed onto a freshly glow-discharged (by Glow discharge cleaning system: PELCO easiGlow™ Glow Discharge System), carbon-coated formvar, copper grid-400mesh (Electron microscopy sciences, #CF400-CU). After 2 min, the sample solution was wicked off with filter paper, the grid rinsed with deionized water, and 5 μl of 2% (wt/vol) phosphotungstic acid stain (pH 7.0) was placed on the grid. After 1 min, the staining solution was wicked away and the grid air-dried. The negatively stained sample was then examined by using Talos L120C (Thermo Fischer Scientific) at an acceleration voltage of 120 kV imaged with 4 k × 4 K Ceta CMOS camera at x45,000. Representative images are shown in Figure S1 a and b.

2.3 | Cell culture

2.3.1 | Culture of HEK293 Flp-In cells

HEK293 Flp-In and the sTREM2-WT expressing HEK293 Flp-In cells were cultured in growth medium GlutaMAX™ (DMEM containing

high glucose [4.5 g/L], phenol red, sodium pyruvate additive, 10 mM HEPES), supplemented with 10% heat-inactivated fetal calf serum (FCS), 1% penicillin and streptomycin (P/S) solution, and 100 μg/ml hygromycin in incubators maintained at 37°C and 5% CO_2 (Ibach et al., 2021). Using the QuikChange-II kit (Agilent Technologies), site directed mutagenesis was carried out according to the manufacturer's instructions in order to introduce the stop codon at aa158 of full length TREM2 construct. The generation of stable cell line was described previously (Ibach et al., 2021). Briefly, the cells were cultured until 70%–80% confluency and washed with DPBS. Co-transfection was carried our using mammalian Flp-In™ host cells with a 9:1 ratio of pOG44 coding for Flp recombinase and pcDNA5/FRT plasmid DNA containing sTREM2 (aa1–aa157) sequence using Lipofectamine 2000 (Thermo Fisher Scientific) in a transfection medium (OptiMEM, Thermo Fisher Scientific). After 24 h, the medium was replaced by medium containing 100 μg/ml Hygromycin B for selection of single cell clones by limiting dilution. Clones were screened by detection of secreted Trem2 in the supernatant.

2.3.2 | Culture of Expi293F™ cells

Expi293F™ cells were grown in suspension with serum free Free-Style™ expression medium (Thermo Fisher Scientific) and were kept at 37°C and 8% CO_2.

2.3.3 | Culture of WT and TREM2^{T66M} primary microglia cells

The cells were isolated by the previously described method (Giulian & Baker, 1986). Briefly, brains from neonatal mice were stripped of the meninges and dissociated using mechanical shearing and trypsin (Life Technologies). Cells of two brains were plated on poly-L-lysine (PLL, Sigma-Aldrich) coated T75 culture flasks (Greiner bio-one) and cultivated in DMEM (Gibco by Thermo Fisher Scientific) supplemented with 10% FCS and 1% P/S (Gibco). On the next day cells were washed three times with DPBS (Gibco) to remove cellular debris and cultured with DMEM supplemented with 10% FCS, 1% P/S and 1% L929 conditioned medium as a source of growth factors. After 7–10 days loosely attached mature microglia were shaken off the astrocytic layer with a repetition of the harvesting procedure all 2–3 days for up to three times. For experiments, primary microglia were seeded on poly-D-lysine (PDL, Sigma-Aldrich) coated glass cover slips at a density of 100,000/well into 24 well plates and allowed to adhere overnight in serum-free DMEM complemented with 1% N-2 supplement (Gibco).

2.4 | TREM2 ectodomain purification

2.4.1 | sTREM2 for the dot blot experiments

For the dot blot assay, cell supernatant from three 15 cm dishes of HEK293 Flp-In controlk or sTREM2-WT expressing HEK293 Flp-In

cells was collected after 24 h of incubation. Saturated solution of ammonium sulphate (AS) was made (3.9 M at 0°C) and the total protein was precipitated with 40% AS solution. Because the addition of AS acidifies the solution, a 1 M Tris–HCl buffer (pH 8.0) was added to the supernatant so that the final concentration was 50 mM (Burgess, 2009; Wingfield, 2001). The mixture is gently mixed and incubated for 1 h on ice and then centrifuged for 30 min at 4°C at 16,000 rcf. The supernatant was discarded and the pellet was resuspended in 5 ml of 1X PBS and this solution was used for dot blot assay (Data S1a for the immunoblot).

2.4.2 | TREM2 ectodomain for BLI studies

A cDNA construct encoding residues aa19–aa143 of TREM2 with a C-terminal His-tag was subcloned into a mammalian expression vector, pHLSec (Aricescu et al., 2006) and transfected into Expi293 cell line using polyethylenimine (PEI) (Backliwal et al., 2008) as the transfection reagent. Endotoxin-free chemicals and plastic ware were used. Recombinant protein was purified from the culture medium using Ni-Excel and size exclusion chromatography followed by Endo H$_f$ (NEB, # P0703L) treatment and the buffer exchange to BLI assay buffer by using Superose$^®$ 6 Increase 10/300 GL (GE Healthcare, #29-0915-96) and the final concentration of the protein was determined by using Biophotometer (Eppendorf) (Vilalta et al., 2021). The obtained TREM2 was detected with Anti-TREM2 antibody (Data S1b for the immunoblot).

2.4.3 | sTREM2-Fc and Fc for pull down experiments

sTREM2-Fc1 vector was generated by inserting human sTREM2 (aa1–aa157) sequence into the pFUSE-hIgG1-Fc1 expression vector. Expression of the Fc-fusion proteins was done following the protocol described by Fang et al. (2017). Briefly, one day before transfection, cells were seeded at 1.5 million viable cells per milliliter (mvc/ml) in fresh medium. The next day cells were transfected at 3 mvc/ml in half of the final volume with a 1 mg/ml linear 40 kDa PEI Max solution (Polysciences, #24765-1) and the respective DNA (1 μg/ml) in a 6:1 ratio. Efficiency of transfection was further increased by addition of 0.1% Pluronic$^®$ F-68 (Thermo Fisher Scientific, #24040032). After 24 h the transfection mix was diluted with fresh medium 1:1 and supplemented with 0.5 M valproic acid (Sigma Aldrich, #VPA P4543) to a final concentration of 3.5 mM. The conditioned media were collected after 4–5 days. Following centrifugation, filtration and pH adjustment the media were loaded on a HiTrap™ Protein G HP 1 ml column and affinity purified via FPLC. Eluted fractions were neutralized by addition of 1 M Tris (pH 9.0). Concentration and buffer exchange against PBS was performed by ultrafiltration with a 10 kDA MWCO column (Sartorius, Göttingen). The concentration of the purified proteins was determined by a spectrophotometer measuring the absorbance at 280 nm (Data S1c for the immunoblot).

2.5 | Dot blot assay

Monomer rich fractions of Aβ were prepared from freshly reconstituted Aβ stocks by dilution to 23 μM in ice cold PBS and ultracentrifugation at 4°C at 100,000*g* for 1 h. Aβ in the supernatant was considered as monomer rich preparation, and characterized by western immunoblot (please refer Figure S1c). Oligomer rich Aβ (oAβ) preparations were obtained as described in Method-1. Then, 2 μl from each of above equimolar preparations from the stock solution (23 μM) were spotted on nitrocellulose (NC) membranes, and the membranes were allowed to dry. The NC membranes were then incubated with concentrated cell supernatant overnight at 4°C. The membranes were washed with TBS-T (3 × 5 min) and then blocked with Odyssey Blocking Buffer (LI-COR Bioscience) for 1.5 h at RT. The membranes were then incubated overnight in primary antibody (monoclonal antibody 4B2A3 for detection of TREM2) at 4°C. The NC membranes were then washed with TBS-T (3 × 5 min) and incubated with LI-COR fluorescent secondary antibody for 1 h at RT, washed with TBS-T (3 × 5 min), then once with TBS (5 min) and imaged with Odyssey® CLx (LI-COR Biosciences). To detect Aβ on the same membranes after detection of bound TREM2, the dot blots were washed with TBS-T (3 × 5 min) followed by incubation with 4G8 antibody overnight to detect Aβ variants. The NC membranes were washed with TBS-T (3 × 5 min) and incubated with LI-COR fluorescent secondary antibody for 1 h at RT, washed with TBS-T (3 × 5 min), then once with TBS (5 min) and developed with LI-COR Odyssey® CLx (LI-COR Biosciences). (please refer Data S1d for the original dot blots cropped for Figure 1b).

2.6 | Bio-layer interferometry (BLI) studies

The aggregation state of the different Aβ variants (prepared by Method-1) was controlled by TEM; (Figure S1a). No significant changes in the size distribution of oligomers formed by unlabeled Aβ, Biotin-LC-Aβ or by mixtures of unlabeled Aβ and Biotin-LC-Aβ (at a ratio of 20:1) was observed (Figure S1b) indicating that the conjugation of Aβ with biotin does not affect the average size of oligomers. Mixtures of Biotin-LC-Aβ with the different N-terminal truncated or post-translationally modified Aβ variants (also at 20:1 ratio) also yielded very similar size distribution of oligomers between 8 and 55 nm. Only the oligomer preparation with pSer8-Aβ also contained larger oligomers with sizes between 55 and 90 nm. This was observed for both, Aβ(1–42) and Aβ(3–42) variants. However, also for pSer8-Aβ variants, >95% of the oligomers were in the size range of 8–55 nm. For BLI studies with TREM2 ectodomain by using Octet RED384 (Forte Bio), we used 5% of Biotin-LC-Aβ(1–42) for mixing with Aβ variants compared with only Biotin-LC-Aβ(1–42) (unpublished data). Further, we optimized the concentration of already mixed oAβ to immobilize onto the biosensors. Initial experiments revealed that 5% of 1 μM Biotin-LC-Aβ mixed with 1 μM of oAβ when immobilized onto the streptavidin (SA) biosensors (Forte Bio #18-0009) showed a similar loading and binding as compared with 100%, 5% Biotin-LC-Aβ (Data S2a,b) and hence the same concentration of mixed Aβ variants

was used in this study. In addition to this, we also checked the differential loading of oAβ onto the SA biosensors in which oAβ(1–42) pSer26 showed higher loading as compared with other variants (Data S2c).

For BLI kinetic measurements, Streptavidin (SA) biosensors were hydrated with 220 μl assay buffer (20 mM HEPES, 500 mM NaCl, 0.1% BSA, 0.02% Tween 20 (pH 7.4) for 30 min (96 well plate). Further, biosensors were exposed to 220 μl buffer in order to determine the initial baseline. The Biosensors were exposed to oligomer rich preparations obtained from mixtures of the respective Aβ variants and Biotin-LC-Aβ in 20:1 ratios. Biosensors were then exposed to 220 μl of assay buffer for 450 s for another baseline measurement. The biosensors were exposed to 220 μl assay buffer containing TREM2 ectodomain at different concentrations (1, 2, 5, and 10 μM) prepared in BLI assay buffer for 60 s to measure association. The biosensors were then exposed to 220 μl of assay buffer for 150 s to measure dissociation. The kinetic constants of BLI were obtained with four different concentrations of TREM2 ectodomain and data was aligned at the y-axis and smoothed by Savitzky–Golay filtering. Curves were processed by adjusting to BLI control buffer, and curve fitting was performed using 2:1 heterogenous ligand as a model due to the heterogenicity of Aβ. KD1 and KD2 values provide the measure of the relative coefficients for dissociation and binding, wherein KD1 measures interaction that occupies the highest percentage of the binding surface area and KD2 characterizes the secondary interaction, determined mathematically by the Octet Data Analysis software.

2.7 | Immunoprecipitation of Aβ using sTREM2-Fc

For assessing differential binding of mAβ and oAβ variants to TREM2, 2 μg of sTREM2-Fc or hIgG1-Fc were pre-coupled to magnetic Protein G beads (SureBeads™, Bio-Rad) for 20 min at 23°C. The coupled beads were then further incubated with 2 μg of the oAβ preparation (prepared by Method-2) for 1 h at 23°C in PBS buffer containing 0.1% Tween-20 (PBS-T). After precipitation and subsequent thorough washing steps, the bound proteins were eluted from the beads by addition of 20 mM glycine solution at pH 2.5. Finally, the eluate was neutralized with 1 M Tris–HCl pH 8 and boiled at 95°C in Laemmli buffer before being subjected to immunoblot analysis. For a quantitative assessment, this protocol was slightly altered by reducing the amount of beads (300 μg) and Aβ (1 μg) while increasing the amount of sTREM2-Fc and hIgG1-Fc to 10 μg to ensure complete saturation of the beads with recombinant protein.

2.8 | SDS-page

Protein separation was performed using the XCell SureLock®Mini-Cell or XCell4 SureLock® Midi-Cell SDS-PAGE system (Invitrogen™, #V601020). Samples prepared in 5x SDS sample buffer and boiled at
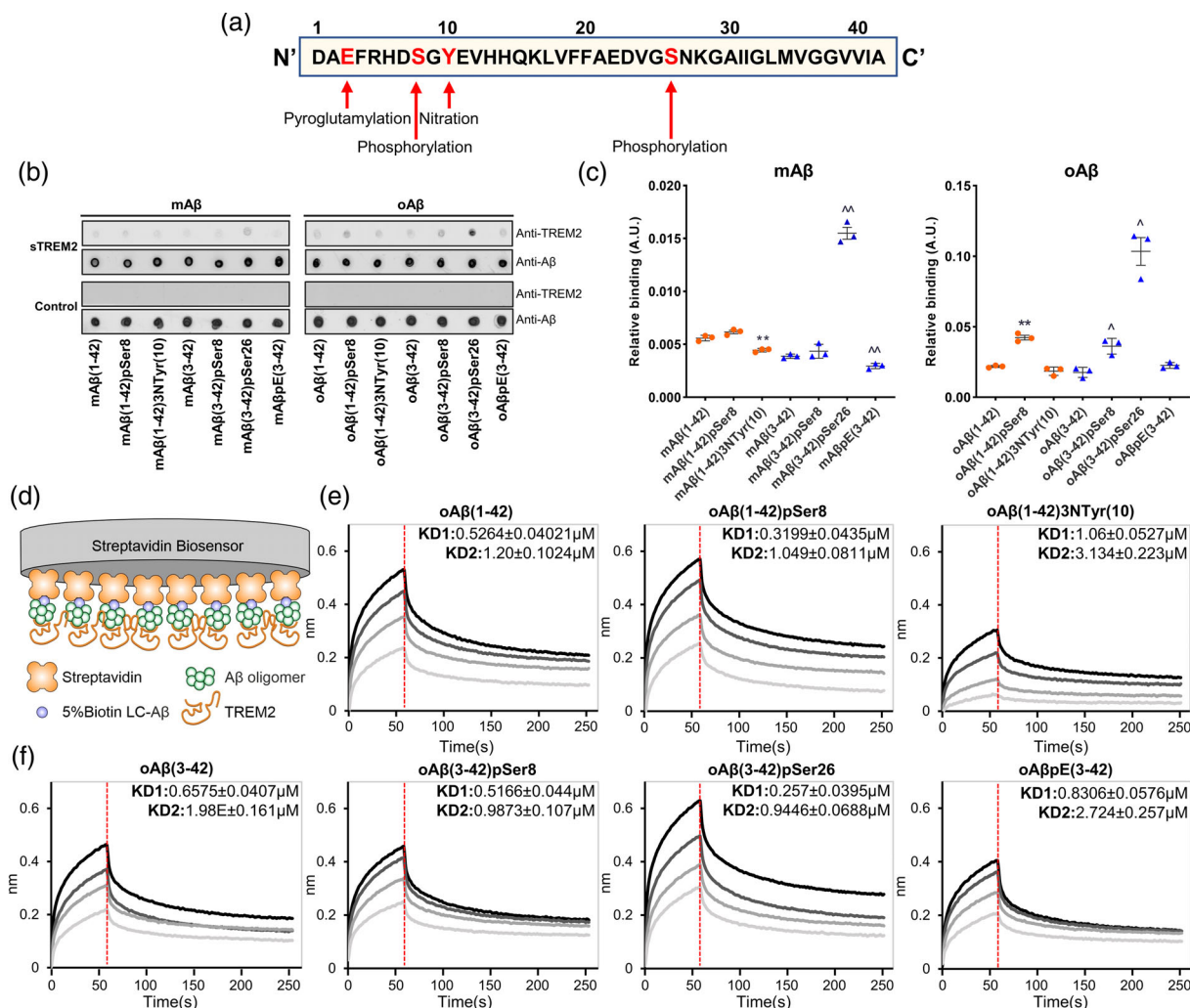
FIGURE 1 Differential interaction of TREM2 with modified Aβ variants. (a) Pictorial illustration of various PTMs of Aβ peptides used for binding assessment in this study. (b) Representative dot blot of various mAβ and oAβ variants spotted on the NC membrane followed by incubation with concentrated supernatant of control HEK293 Flp-In cells or transgenic sTREM2 expressing stable HEK293 Flp-In cells. (c) Quantification of ratio of signal intensity of sTREM2 detected with anti-TREM2 antibody and respective Aβ variants detected with 4G8 antibody. The average values of ratio from experimental triplicate of Aβ(1–42) variants are represented as "●" while of Aβ(3–42) variants are represented as "▲." * or ˆ represents a comparison of Aβ(1–42) or Aβ(3–42) variants respectively. (n = 3, unpaired *t* test with Welch correction, *or ˆ $p < .05$, **or ˆ $p < .01$). (d) Schematics of BLI strategy using streptavidin (SA) biosensors. Biotinylated oAβ variants immobilized on SA biosensor to assess the interaction with TREM2 ectodomain at concentrations of 1, 2, 5, 10 μM. (e, f) Representative association/dissociation curves of varying TREM2 ectodomain concentrations and calculated KD1/KD2 values of TREM2 ectodomain binding with oAβ variants (see Table S1 for other set of values). $n = 2$, which includes repetition of the entire experiment including preparation and dilution of oAβ oligomers, KD-equilibrium dissociation constant

95°C for 5 min were separated according to their molecular weight on a precasted discontinuous Bis-Tris NuPAGE Novex 4%–12% gel (Invitrogen™, #V601020). Separation was achieved by using 1x NuPAGE™ MES SDS Running Buffer and a constant voltage of 120 V for 1 h. Gels were subsequently analyzed by western immunoblot analysis (Ibach et al., 2021; Kumar et al., 2021).

2.9 | Western immunoblotting

Proteins separated by SDS-PAGE were transferred to NC membranes as described previously (Ibach et al., 2021), at constant current of 400 mA and for 2 h. The membranes were then blocked for 1 h at constant agitation with a 5% milk solution, followed by incubation of the membrane

over night at 4°C and constant agitation (orbital shaker) with a solution of the primary antibody in 1x TBS-T. The next day, the membranes were washed (3 × 5 min) followed by incubation with respective secondary antibody conjugated either to horseradish peroxidase or a fluorophore for 1 h at RT. The membranes were washed again (3 × 5 min) followed by detection of the protein with the Chemidoc XRS Imager (BioRad) or Odyssey® CLx (LI-COR Biosciences).

2.10 | Binding and phagocytosis assays

oAβ variants prepared as described in Method 2 were incubated with primary microglia from WT or TREM2[T66M] transgenic mice. Cells were incubated with 1 μM of Aβ oligomers in DMEM GlutaMAX™ at 37°C

and 5% CO_2 for 2 h before they were fixed, permeabilized and stained. Coverslips were mounted on glass slides and observed using a VisiScope CSU-W1 spinning disk confocal microscope. As a control, cells were also pretreated with DMSO at a final concentration less than 0.01% and 10 μM Cytochalasin D (CytoD) dissolved in DMSO, keeping the final concentration of DMSO less than 0.01% for 30 min to block actin polymerization and thereby macropinocytosis before changing to the assay conditions described before (Kim et al., 2017; Xiang et al., 2016).

In order to assess the binding of oAβ variants prepared as described in Method-2, primary microglia from WT and TREM2[T66M] transgenic mice seeded as described above were treated with 1 μM of oAβ in DMEM GlutaMAX™ and incubated on ice for 2 h followed by fixation and staining. In order to assess the uptake of bound Aβ, primary microglia were first incubated with 1 μM of oAβ in DMEM GlutaMAX™ on ice for 2 h. After this, the cells were washed and further incubated at 37°C and 5% CO_2 for 2 h. The cells were then fixed, permeabilized and stained.

2.11 | Immunocytochemistry of primary microglia

Cells were fixed for 15 min in 4% paraformaldehyde (PFA) before permeabilization with 0.1% Triton-X100 (PBS) for 5 min. After blocking with 3% BSA in PBS-T, 100 μl of primary antibody in 1% BSA was added to each coverslip and incubated at RT for 1 h. Coverslips were subsequently washed three times with 0.5% BSA in PBS-T. Afterwards, respective secondary antibodies in 1% BSA solution were added and coverslips were incubated for 1 h at RT in the dark, followed by another three washing steps. Finally, the coverslips were mounted on a microscopy slide using VECTASHIELD® antifade mounting medium with DAPI (Vector lab, #H-1200).

2.12 | Transgenic mice

Wild-type and homozygous TREM2[T66M] crossed to APPKM670/671NL; PS1ΔE9 transgenic mice were obtained from Taconic Biosciences GmbH, and were all of the C57BL/6 genetic background. Mice were housed under standard conditions at 22°C and a 12 h light–dark cycle with free access to food and water. Animal care and handling of these mice was performed according to the Declaration of Helsinki and approved by the local ethical committees (LANUV NRW 84–02.04.2017.A226).

APP695KM670/671NL; PS1L166P transgenic mice with endogenous TREM2 or the TREM2 deletion (TREM2^{−/−}) mice were described previously (Parhizkar et al., 2019; Turnbull et al., 2006).

2.13 | Immunofluorescence analysis of mouse brains

Mouse brain samples were processed as described previously (Kumar et al., 2021; Parhizkar et al., 2019), and 20–25 μm sections

collected in PBS for staining. For immunofluorescence (IF) staining, heat-induced sodium citrate antigen retrieval (pH 6.0) using 10 mM sodium citrate with 0.05% Tween-20 at 95°C for 30 min or 80% formic acid treatment for 8 min (Gerth et al., 2018) was employed depending on various Aβ species. Sections were then washed once with PBS. For X-34 staining, sections were treated with 100 μM of X-34 prepared in 60% PBS/40% EtOH mix (pH was adjusted with 1 M NaOH) for 10 min at RT (Parhizkar et al., 2019; Styren et al., 2000). The sections were washed briefly with 60% PBS/40% EtOH and subjected to permeabilization with 0.3% Triton X-100 for 30 min before blocking for 2 h in 5% NHS and 2.5% BSA prepared in 1xPBS. Mouse on Mouse Blocking Reagent (Vector laboratories, #MKB-2213) was used for primary antibodies generated in mouse or rat at a dilution of 1 drop/1000 μl. Primary antibodies (Table S2) were added and the sections kept at 4°C overnight. After adding the appropriate secondary antibodies (Table S2), tissue sections were mounted onto slides by using VECTASHIELD® Hardset™ antifade mounting medium (Vector lab, #H-1400) or VECTASHIELD® antifade mounting medium with DAPI (Vector laboratories, #H-1200).

2.14 | Confocal imaging and data analysis

Images were acquired using VisiScope CSU-W1 spinning disk confocal microscope and VisiView Software (Visitron Systems GmbH). Laser and detector settings were maintained constant for the acquisition of each immunostaining. For all analyses, at least two images were acquired using x20, x40W or x63W (W: water immersion) objective at 2048 × 2048 pixels, with z-step size of 1 μm.

For quantification of microglial binding and uptake of Aβ, IntDen was calculated by manually drawing border around randomly selected Aβ positive microglia. Representation of ratio of Aβ positive microglia/total microglia was done by manually counting Aβ positive cells and automatically counting DAPI positive total cells for 10 images/experiment (5 images per coverslips and the experiments were in duplicates).

For analysis of internalized pSer26-Aβ in transgenic mouse brain, number of plaque associated microglia were manually counted in 500 × 500 μm areas of somatosensory cortex (SSC) on 1–2 independently stained sections and then represented as the ratio of pSer26-Aβ positive microglia/total Iba1 positive microglia.

2.15 | Statistical analysis

Statistical analyses were performed using Prism (GraphPad Software). Unless otherwise stated, two-sided, unpaired student's t tests with Welch's correction was used to determine the statistical difference between groups in analyses that only required single comparisons. The degree of significance between groups is represented as *$p < .05$, **$p < .01$, ***$p < .001$, ****$p < .0001$, and [ns]$p > .05$.

2.16 | Randomization and blinding

The primary microglia experiments and the immunofluorescence analysis of mouse brains were initially performed blinded with coded slides. However, complete randomization was not possible with the stainings of mouse brain sections with a microglial marker depicting microglial clustering. Following the completion of the analysis, the groups were unblinded to perform statistics.

2.17 | Data collection

The BLI data were acquired and analyzed by using Octet RED384 and data analysis 9.0 (Forte Bio). The TEM images were acquired by using Talos L120C (Thermofischer Scientific). Confocal images were acquired by using VisiScope CSU-W1 spinning disk confocal microscope and VisiView Software (Visitron Systems). The western immunoblotting data were acquired by using by enhanced chemiluminescence using Chemidoc XRS Imager (BioRad) or Odyssey® CLx (LI-COR Biosciences). Microsoft Excel was used to organize and to calculate the averages of each repeated experiment. Graph Pad (Prism v7.0) was used to build graphs and perform statistical analyses presented throughout the manuscript.

3 | RESULTS

3.1 | Differential binding of TREM2 to post-translationally modified Aβ species

In order to investigate the interaction of TREM2 with different Aβ species (Figure 1a), we first assessed the binding of soluble TREM2 (sTREM2) to monomeric (mAβ) and oligomeric (oAβ) forms of distinct post-translationally modified and non-modified Aβ variants in dot blot assays. For this, different Aβ variants in monomeric and oligomeric form were spotted onto Nitrocellulose (NC) membranes and incubated with sTREM2 obtained from conditioned media of transgenic cells expressing a TREM2 variant with a stop codon at position 158 thereby representing the soluble TREM2 ectodomain that is physiologically generated by proteolytic processing of full-length TREM2 (Feuerbach et al., 2017; Schlepckow et al., 2017; Thornton et al., 2017; Wunderlich et al., 2013). sTREM2 bound to the different Aβ species was detected by an anti-TREM2 antibody (4B2A3). This antibody recognizes an epitope within the stalk region of TREM2 (aa 131–148) (Ibach et al., 2021), thereby avoiding possible competition with ligands bound to the ligand binding domain of sTREM2. Consistent with previous reports, TREM2 showed strongly increased interaction with oligomeric as compared with monomeric Aβ variants (Figures 1b,c and S1). Oligomers formed by Aβ variants phosphorylated at Ser8 (pSer8-Aβ) or Ser26 (pSer26-Aβ) showed significantly increased interaction with TREM2 as compared with non-modified, nitrated or pyroglutamate-modified variants. With monomeric forms, pSer26-Aβ also showed strongly increased binding to TREM2 as

compared to non-modified Aβ or otherwise modified Aβ variants. However, it should be noted that pSer26-Aβ has the highest tendency to form oligomeric assemblies (Kumar et al., 2016), and it cannot be excluded that pSer26-Aβ formed some oligomeric assemblies during this assay.

To validate these findings with an independent method, we utilized BLI (Figure 1d). The different Aβ variants were mixed with Biotin-labeled-Aβ at a ratio of 20:1 and oligomerized as described previously (Vilalta et al., 2021). Oligomer preparations were immobilized on streptavidin biosensors (Figure 1d) and kinetic binding assays performed using purified TREM2 ectodomain at different concentrations (1, 2, 5, and 10 μM). BLI kinetic studies also revealed increased binding of the TREM2 ectodomain to oligomers that contained pSer8-Aβ or pSer26-Aβ (Figure 1e,f). The lowest binding was measured for nitrated Aβ3NTyr(10) as compared with non-modified Aβ (Figure 1e). Oligomeric pyroglutamate modified Aβ (pEAβ) also showed lower binding to the TREM2 ectodomain as compared with non-modified Aβ. (Figure 1f, Table S1).

Pull-down assays from mixtures containing monomeric and oligomeric forms of Aβ using sTREM2-Fc fusion proteins further demonstrated that sTREM2 preferentially binds to oligomeric Aβ assemblies. Again, highest binding was detected for phosphorylated Aβ oligomers as compared with non-modified Aβ species (Figure 2a,b). The combined data from different biochemical and biophysical assays demonstrate that phosphorylation of Aβ at Ser8 or Ser26 increased binding to TREM2 in particular for oligomeric Aβ assemblies.

3.2 | TREM2 dependent binding and phagocytosis of modified Aβ species by primary microglia

To further characterize the interaction of Aβ species with TREM2 and its functional implications, we used primary microglia from wild-type (WT) mice expressing endogenous TREM2 and mice with the TREM2[T66M] knock-in (KI) mutation. The TREM2[T66M] mutation is associated with Nasu Hakola disease (NHD) or frontal lobe dementia (FTD) and strongly impairs ectodomain folding and cell surface transport of the receptor thereby causing a loss of function (Kleinberger et al., 2014; Le Ber et al., 2014). First, we assessed the binding of phosphorylated and non-modified Aβ species to the plasma membrane of primary microglia from WT mice by incubation of cells on ice to halt endocytosis (Tamboli et al., 2008; Wesen et al., 2017). While the membrane-association of pSer8-Aβ was lower, that of pSer26-Aβ was increased as compared with binding of non-modified Aβ (Figure 3a,b), indicating phosphorylation-site and phosphorylation-state specific interaction of Aβ with the microglial surface. Decreased binding of pSer8-Aβ was observed for the two length variants of Aβ, 1–42 and 3–42. Since Aβ(1–42)pSer26 could not be chemically synthesized, the analysis was restricted to Aβ(3-42)pSer26 and compared with non-modified Aβ(3–42) and Aβ(3-42)pSer8 species, respectively. Importantly, binding of the different Aβ species was reduced by about 50% in TREM2[T66M] expressing microglia as compared with TREM2 WT expressing microglia (Figure 3a,b). On one hand, these results
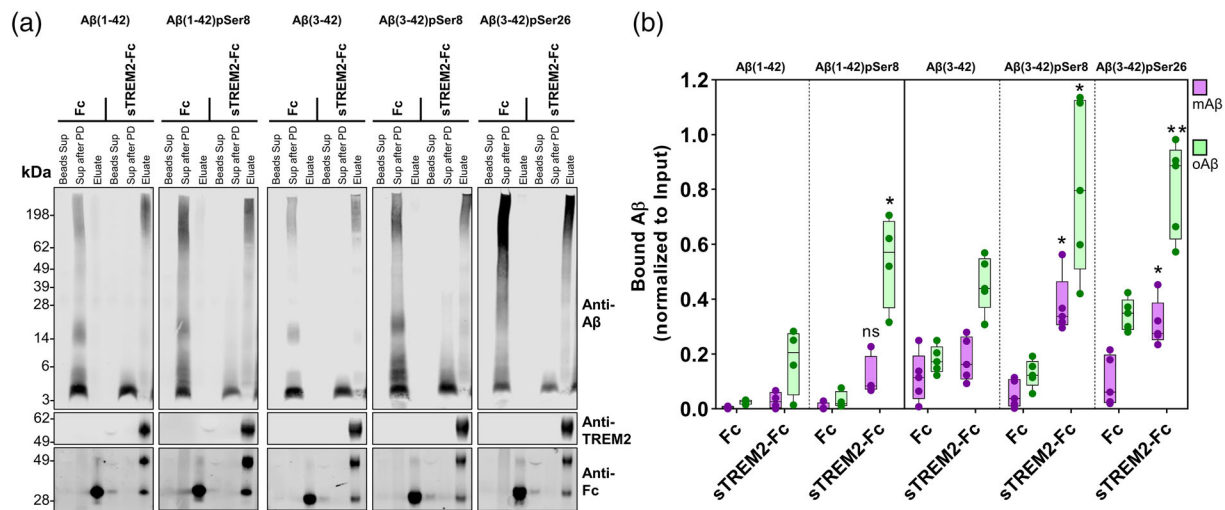
FIGURE 2 Increased interaction of TREM2 with oligomeric phosphorylated Aβ variants. (a) Representative western immunoblot of samples from pull-down (PD) experiments for oAβ with sTREM2-Fc or with Fc alone as a control. Efficient pre-coupling of sTREM2-Fc or Fc alone to protein-G magnetic beads is confirmed by the depletion of these proteins from the buffer solution in the supernatant after pre-incubation of beads ("Beads sup" lanes). A preferential pull-down of oAβ by sTREM2 is indicated by robust signals for aggregated forms of Aβ in the "Eluate" fractions detected in the upper regions of the gels, while large portions of mAβ remains in the supernatant after the pull-down ("Sup after PD"). (b) Box and whiskers plot of IntDen of signals for the monomer band or oligomeric forms. Values were normalized to the respective input. Each dot represents an independent experiment. All data represent mean ± SEM ($n = 4$ for Aβ(1–42) or $n = 5$ for Aβ(3–42) variants, unpaired t test with Welch correction, $*p < .05$, $**p < .01$, $^{ns}p > .05$)

demonstrate the involvement of functional TREM2 in the binding of the different Aβ species, and on the other hand, support previous reports showing that the association of Aβ to microglia could also involve additional proteins or lipids present at the cell surface (Verdier et al., 2004; Yu & Ye, 2015). When cells were further incubated at 37°C upon binding of Aβ to the surface, we observed differential uptake of bound Aβ depending on the phosphorylation state (Figure 3c,d). While the amount of internalized pSer8-Aβ was lower, the amount of internalized pSer26-Aβ was higher as compared with that of unphosphorylated Aβ. In addition, the number of Aβ positive microglia was lower for pSer8-Aβ exposed cells, but higher for pSer26-Aβ exposed cells as compared with the number of microglia that internalized unphosphorylated Aβ (Figure S2a,b). The phosphorylation-state dependent internalization of Aβ variants in TREM2 WT microglia might involve differences in the aggregation and/or conformation of pSer8-Aβ and pSer26-Aβ (Kumar et al., 2011; Kumar et al., 2012; Kumar et al., 2016). Phosphorylation-state dependent uptake of Aβ was also observed when cells were exposed to Aβ without a precedent binding period, and was reduced by cytochalasin D, indicating the involvement of phagocytosis (Figures 4a,b and S2). Again, the phagocytosis of the different Aβ species was strongly reduced in microglia from TREM2[T66M] KI mice, demonstrating that the differential uptake of phosphorylation-state variants of Aβ depends on functional TREM2 (Figure 4). Co-staining with Lamp-1 revealed partial localization of internalized Aβ in lysosomal compartments (Figures 3 and 4). Lysosomal localization was particularly pronounced for pSer26-Aβ, indicating lysosomal accumulation of this phosphorylated Aβ form. These results indicate that the phosphorylation state of Aβ affects its TREM2 dependent binding and

phagocytosis by microglia. However, in addition to the differential interaction with TREM2, peculiar differences in the aggregation characteristics and conformation of the phosphorylation-state variants of Aβ could contribute to the differential interaction and uptake by microglia.

## 3.3 | TREM2 deletion leads to altered deposition of phosphorylated Aβ variants

To further investigate the role of TREM2 in the interaction of different phosphorylated Aβ species with microglia in vivo, we used APP transgenic mice that express endogenous TREM2 or mice with a TREM2 knockout mutation. Similar to previous studies (Wang et al., 2015; Yuan et al., 2016; Zhao et al., 2018), we also observed decreased microglial clustering around X-34 positive plaques in brains of TREM2^{−/−} mice as compared with TREM2^{+/+} mice (Figure 5a,b). Interestingly, mice homozygous for the TREM2[T66M] mutation also showed reduced clustering around X-34 positive plaques that contain fibrillar Aβ (Figure 5c,d). Immunostaining of brain sections with antibodies against the microglial marker protein Iba1 together with phosphorylation-state specific antibodies for Aβ with Ser8 in phosphorylated or non-modified state (nmAβ) revealed that X-34 positive plaques also contained Ser8-phosphorylated and unphosphorylated (nmAβ) species that are surrounded by microglia in TREM2 WT mice (Figure 5). In contrast, brains of TREM2^{−/−} (Figure 5a,b) or TREM2[T66M] expressing mice (Figure 5c,d) showed increased radial extensions of fibrillar Aβ that are intermingled with microglial processes thereby forming
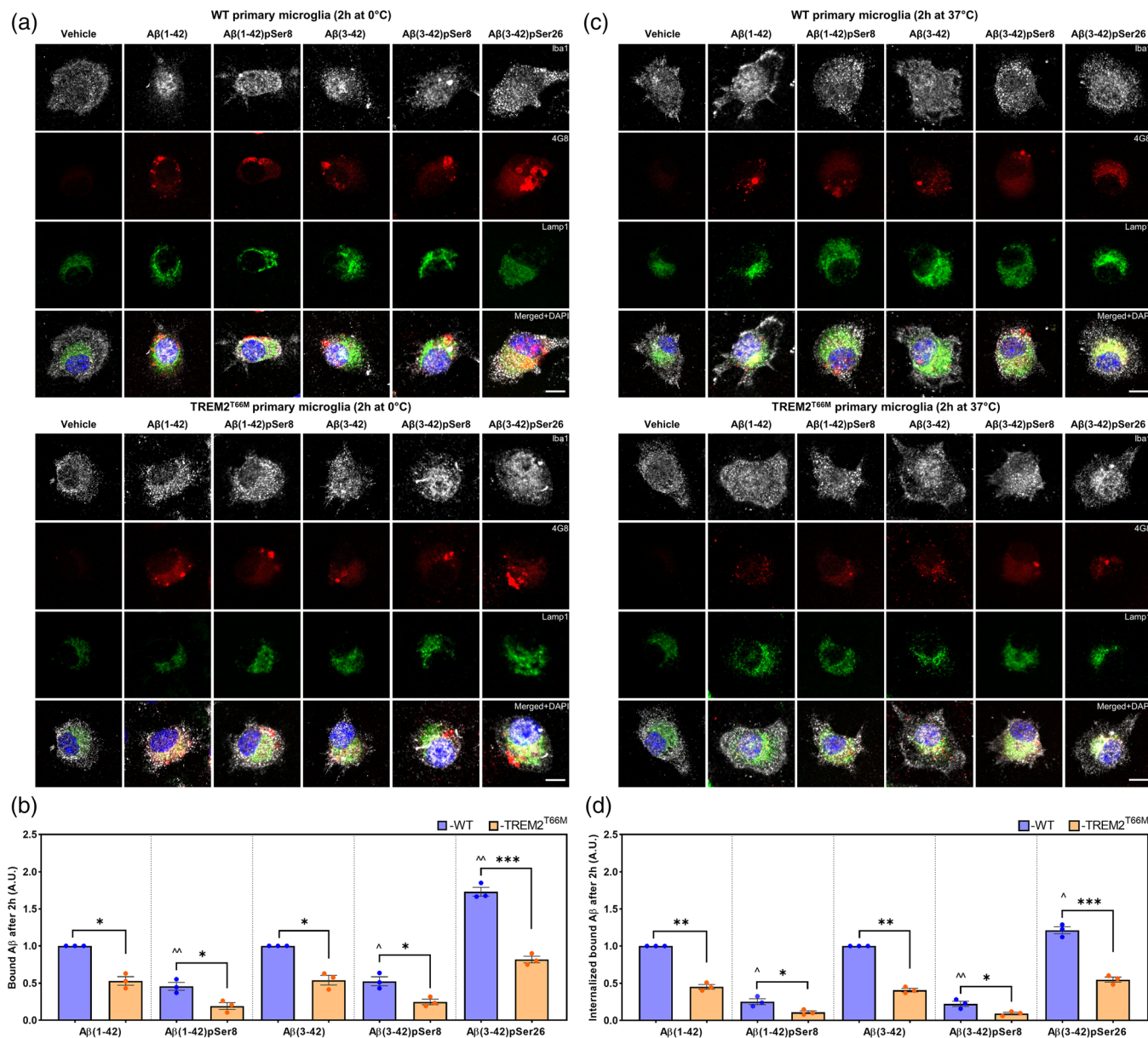
FIGURE 3 Involvement of functional TREM2 in surface binding and subsequent uptake of phosphorylated Aβ variants by primary microglia. (a) Representative immunocytochemical staining images of primary microglia from wild-type (WT) and TREM2^T66M mice, and (b) plot showing the normalized IntDen of oAβ positive cells after treatment with 1 μM oAβ for 2 h at 0°C followed by fixation and staining. (c) Representative immunocytochemical staining images of primary microglia from WT and TREM2^T66M mice, and (d) plot representing the uptake of bound oAβ levels calculated from IntDen of oAβ positive cells after treatment with 1 μM oAβ variants for 2 h at 0°C, followed by washing and incubating at 37°C for 2 h followed by fixation and staining. Microglial cells were stained using Iba1 antibody (white) while Aβ was stained via the generic antibody 4G8 (red). Lamp1 antibody was employed as a lysosomal marker (green) (Scale bar = 10 μm, 63xW). IntDen of oAβ (either 1–42 or 3–42) for WT primary microglia was set as 1 for normalization of values for pSer8 and pSer26-phosphorylated oAβ species and accordingly values for TREM2^T66M were calculated. Each dot represents the average value of normalized IntDen/experiment. Data represent mean ± *SEM* (*n* = 300 cells/group, experimental *n* = 3, unpaired *t* test with Welch correction, *^or ^p < .05, **^or ^p < .01 ***p < .001 for comparison of WT and TREM2^T66M, A.U.-arbitrary units). ^represents comparison of phosphorylated Aβ variants with Aβ (1–42 or 3–42) treated to WT primary microglia

mesh-like structures with various degrees of compaction (indicated by arrow heads, Figure 5). Very similar observations on the morphology of Aβ deposits and interactions with microglia in brains of TREM2^+/+ and TREM2^−/− mice were also made when Aβ was detected by a monoclonal antibody (82E1) that detects the N-terminus of Aβ independent on its phosphorylation state (Figure S3). These findings are consistent with the function of TREM2 to restrict plaque size or growth (Wang et al., 2015; Yuan et al., 2016). It is important to note that TREM2 positive plaque associated microglia also restrict pSer8-Aβ deposits, which could

(a)

(b)
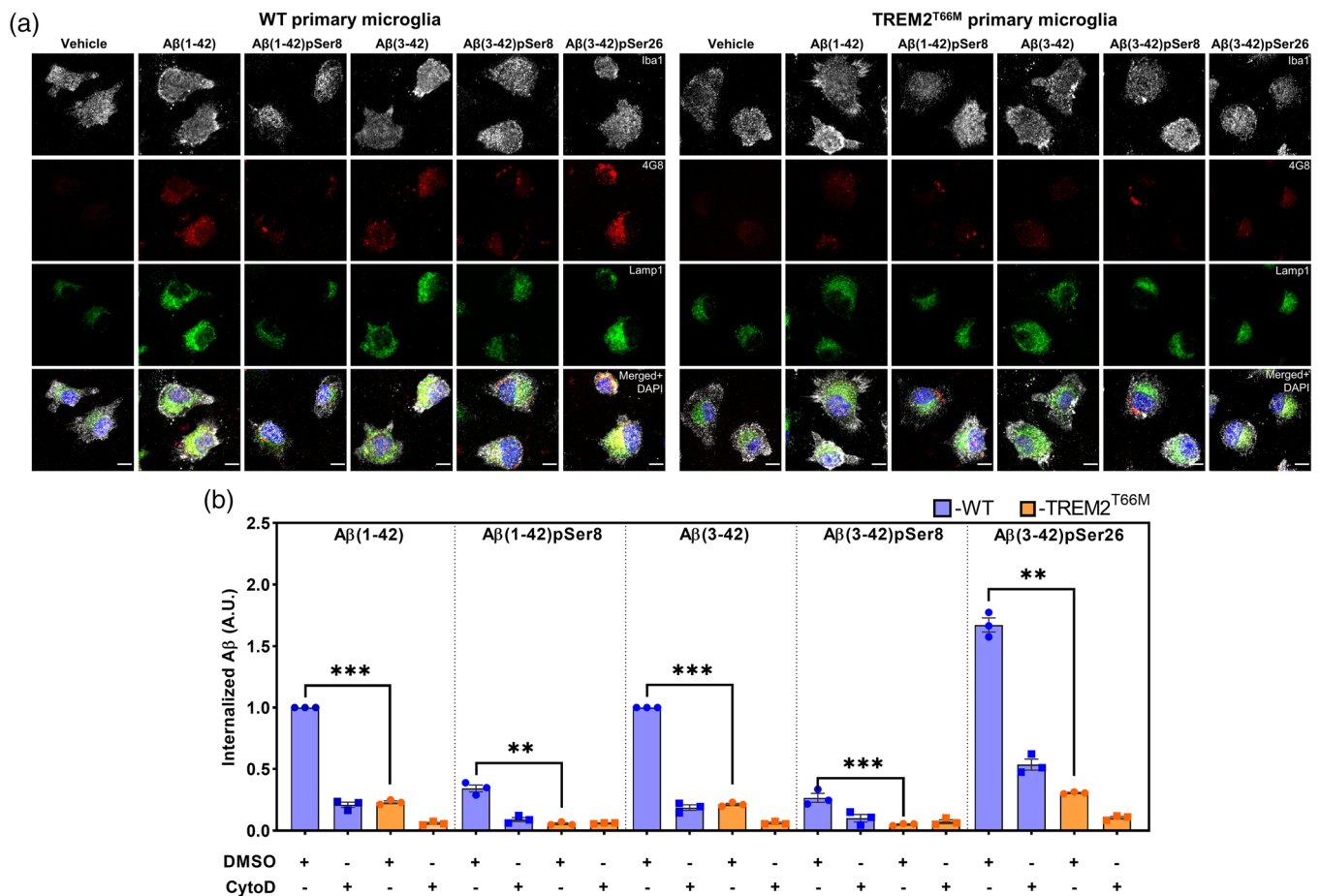
FIGURE 4 Differential phagocytosis of phosphorylated Aβ variants by primary microglia. (a) Representative immunocytochemical staining images of primary microglia from wild-type (WT) and TREM2^{T66M} mice after pretreatment with vehicle (DMSO) or CytoD (Figure S2a) treatment for 30 min followed by treatment with 1 μM oAβ for 2 h at 37°C. Microglial cells were stained using Iba1 antibody (white), and Aβ by antibody 4G8 (red). Lamp1 antibody was employed as a lysosomal marker (green) (Scale bar = 10 μm, 63xW). (Scale bar = 10 μm, 63xW). (b) Plot representing the internalization of different oAβ variants by primary microglia from WT and TREM2^{T66M} mice calculated by the IntDen of internalized Aβ. Each dot represents the average value of normalized IntDen of Aβ positive microglia/experiment. Data represent mean ± *SEM* ($n = 300$ cells/group, experimental $n = 3$, unpaired *t* test with Welch correction, ** $p < .01$, *** $p < .001$ for comparison of WT and TREM2^{T66M}, A.U.-arbitrary units)

be due to enhanced TREM2 binding. However, little if any pSer8-Aβ was detected within microglia (Figure 5a,c).

In contrast to pSer8-Aβ, pSer26-Aβ was abundant within microglia (Figure 6), consistent with the observed increased binding and TREM2-dependent internalization by microglia (see Figures 1–4). Deposition of pSer26-Aβ was detected in the two independent APP transgenic mouse models used in this study (Figure 6). However, in contrast to fibrillar Aβ detected by X-34 or pSer8-Aβ, pSer26-Aβ species were only faintly detected in the core of dense Aβ plaques and rather appeared as small deposits in close proximity of extracellular plaques (Figure 6a,c). Co-immunostaining of pSer26 with Iba1 and Lamp1 revealed lysosome associated pSer26-Aβ within plaque associated microglia in the different APP transgenic mouse models expressing TREM2$^{+/+}$, that was strongly reduced in APP transgenic mice deficient of TREM2 (Figure 6a,b) or expressing the TREM2^{T66M} KI mutation (Figure 6c,d).

4 | DISCUSSION

Here, we show the differential interaction of TREM2 and post-translationally modified Aβ species with oligomers formed by phosphorylated Aβ variants binding most avidly to TREM2. In addition, our data demonstrate the involvement of TREM2 in the binding and uptake of distinct phosphorylation-state variants of Aβ by microglia in vitro and in vivo.

Alternative proteolytic processing of APP and post-translational modifications results in the formation and deposition of a variety of Aβ peptides during the pathogenesis of AD (Barykin et al., 2017; Kummer & Heneka, 2014). Among the different modifications, phosphorylation at Ser8 promotes the fibrillization of Aβ, while phosphorylation at Ser26 rather decreases fibrillization, but stabilizes oligomeric assembly (Kumar et al., 2011; Kumar et al., 2016; Rezaei-Ghaleh et al., 2016). In addition, the phosphorylation at Ser8 increased the stability of Aβ against degradation by microglial cells (Kumar
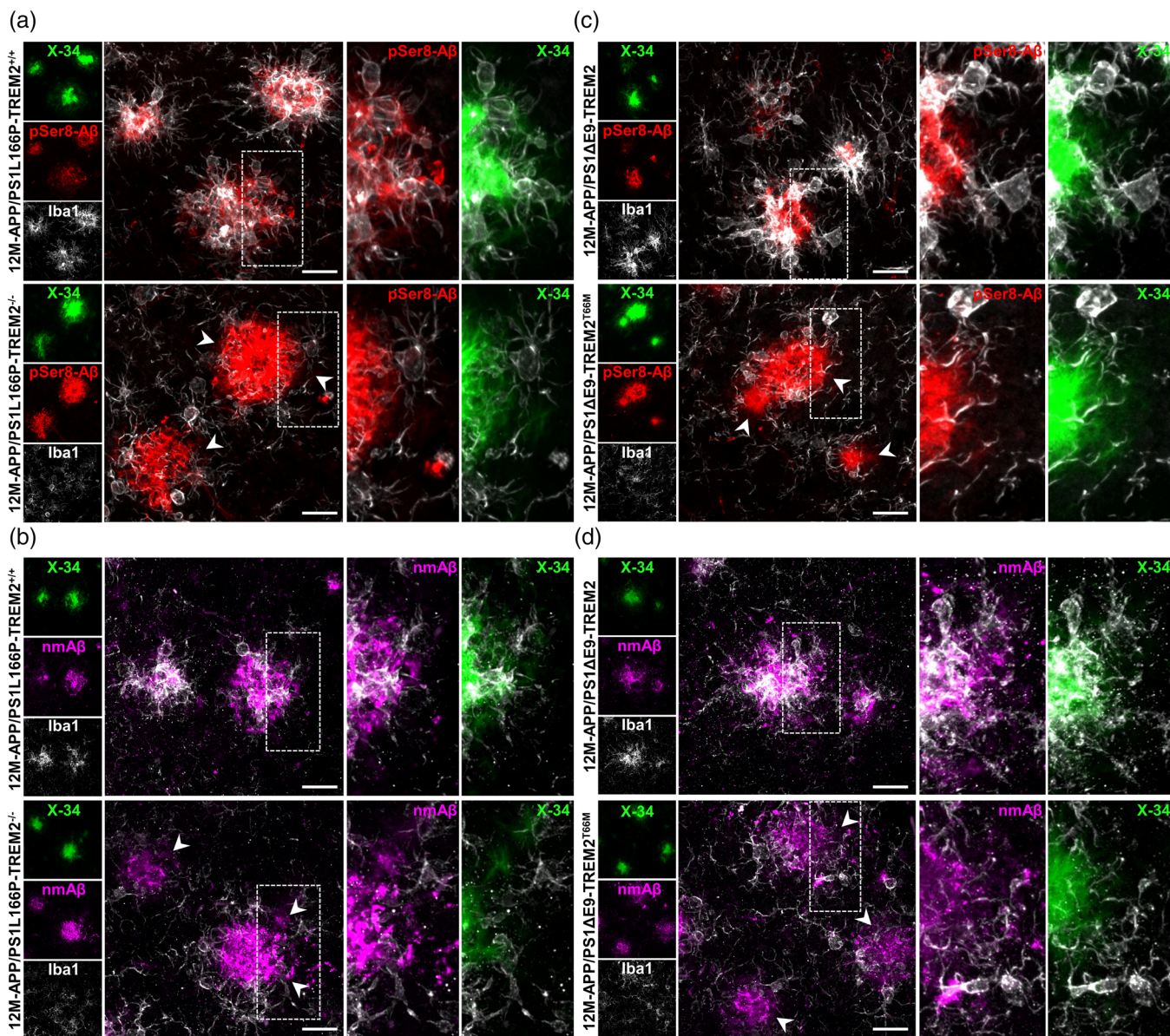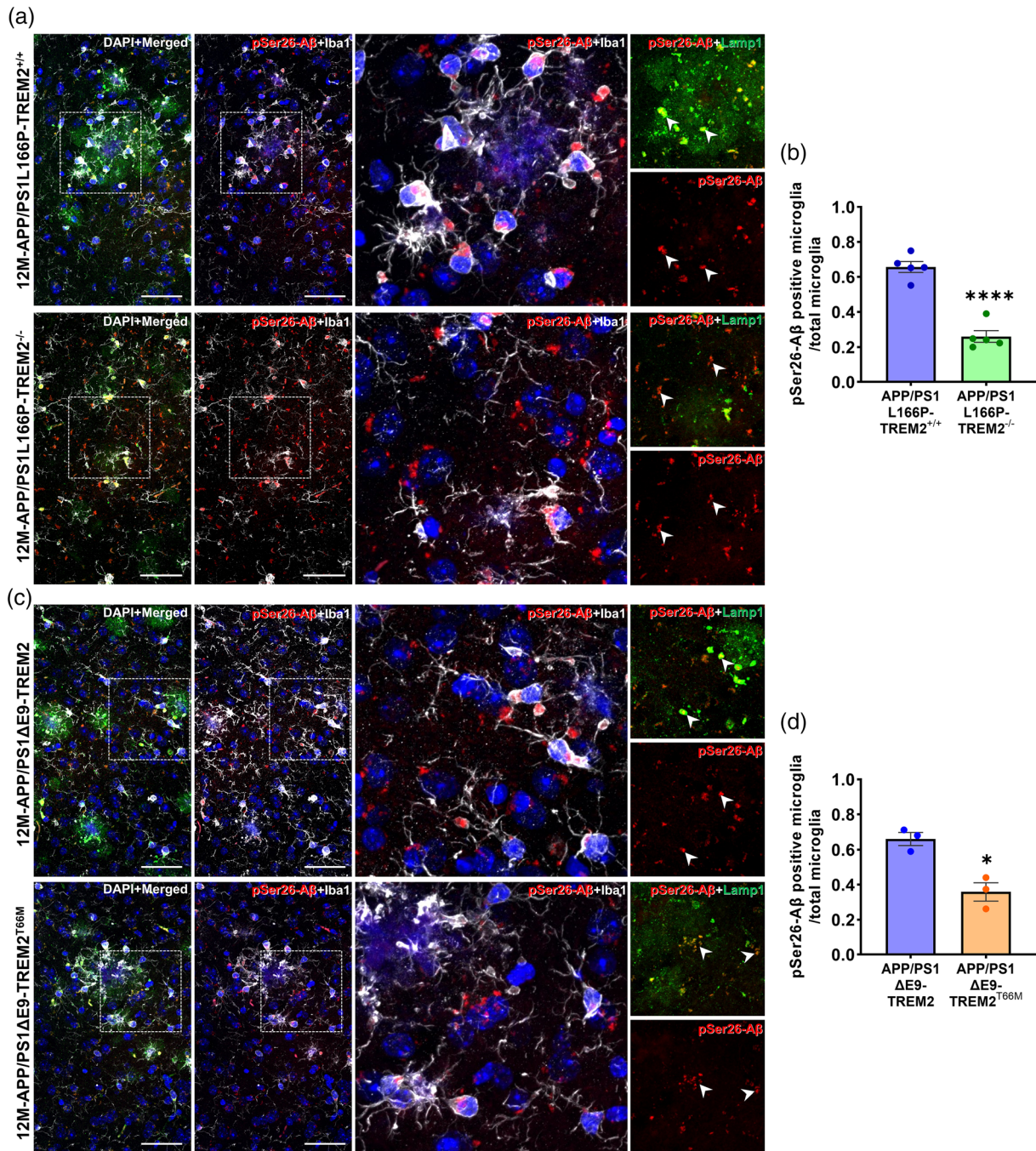
FIGURE 5 Decreased microglial barrier function alters deposition of pSer8-Aβ and nmAβ in brains of TREM2 deficient mice (a, b) Representative IF images of extracellular plaques stained for pSer8-Aβ (a) and nmAβ (b) in 12 M-APP/PS1L166P-TREM2$^{+/+}$ and TREM2$^{-/-}$ mice. Fibrillar Aβ was detected by X-34 and microglia were stained with Iba1. (c, d) Representative IF images of extracellular plaques stained for pSer8-Aβ (c) and nmAβ (d) in 12 M-APP/PS1ΔE9-TREM2 and APP/PS1ΔE9-TREM2^{T66M} mice. Fibrillar Aβ was detected by X-34 and microglia were stained with Iba1. Dotted white boxes indicate the area shown at higher magnification while the arrowheads indicate the mesh-like structures that surround the plaques of varying compaction in TREM2$^{-/-}$ or TREM2^{T66M} mice. (Scale bar = 20 μm, 40xW)

et al., 2012). pSer8-Aβ could also seed aggregation of unphosphorylated Aβ (Hu et al., 2017; Kumar et al., 2011). Consistent with previous findings, we found that TREM2 binds much stronger to oligomeric Aβ assemblies than to monomeric Aβ (Lessard et al., 2018; Zhao et al., 2018). Furthermore, despite having distinct aggregation kinetics and stability, both phosphorylated Aβ species in oligomeric form showed the strongest interaction with TREM2.

We also show phosphorylation-state and phosphorylation-site specific uptake of Aβ by primary microglia. Notably, while the uptake of pSer8-Aβ was decreased, the internalization of

pSer26-Aβ was increased as compared with that of non-modified Aβ. The uptake of all Aβ species was significantly reduced in microglia expressing the TREM2^{T66M} loss of function mutation that is associated with NHD and frontal lobe degeneration (Guerreiro, Bilgic, et al., 2013; Guerreiro, Lohmann, et al., 2013; Paloneva BM et al., 2001). This mutation causes misfolding and strongly decreases the expression of TREM2 at the cell surface (Kleinberger et al., 2014). Thus, these data indicate that cell surface localized TREM2 is important for the regulation of Aβ phagocytosis. However, additional components of the microglial surface,

FIGURE 6 Loss of TREM2 function leads to decreased microglial pSer26-Aβ deposits in brains of TREM2 transgenic mice. (a) Representative IF images of SSC regions of 12 M-APP/PS1L166P-TREM2$^{+/+}$ and TREM2$^{-/-}$ mice co-stained for pSer26-Aβ along with the lysosomal marker Lamp1, and the microglial marker Iba1 (Scale bar = 50 μm, 40xW, dotted white boxes indicate the area shown at higher magnification). (b) Quantification of microglia per cortical region of interest (ROI) showed a decreased number of pSer26-Aβ positive microglia (indicated with arrowheads) in the 12 M-APP/PS1L166P-TREM2$^{-/-}$ compared with TREM2$^{+/+}$ mice ($t[7.976] = 8.615$, ****$p < .0001$). (c) Representative IF images of pSer26-Aβ stained SSC of 12 M-APP/PS1ΔE9-TREM2 and TREM2^{T66M} mice along with the lysosomal marker, Lamp1 and microglial marker, Iba1 (Scale bar = 50 μm, 40xW, dotted white boxes indicate the area shown at higher magnification). (d) Quantification of microglia per cortical region of interest (ROI) showed a decreased number of pSer26-Aβ positive microglia (indicated with arrowheads) in the 12 M-APP/PS1ΔE9-TREM2^{T66M} compared with APP/PS1ΔE9-TREM2 mice ($t[3.577] = 4.739$,*$p = .0118$). All data represent mean ± *SEM*. ($n = 5$ animals (6b) or $n = 3$ animals (6d), unpaired t test with Welch correction)

including receptor proteins and membrane lipids could also be involved in the interaction and uptake of different Aβ variants (Mandrekar et al., 2009; Verdier et al., 2004; Yu & Ye, 2015). In addition, peculiar effects of phosphorylation at Ser8 and Ser26 on the conformation and aggregation of Aβ could also contribute to the differential interaction with TREM2 and handling of the peptides by microglia (Kumar et al., 2011; Kumar et al., 2012; Kumar et al., 2016).

To assess the role of TREM2 in the deposition of phosphorylated Aβ species in vivo, we used two different APP/PS1 transgenic mouse models crossed to TREM2 WT, TREM2$^{-/-}$ mice or TREM2^{T66M} mice. Consistent with previous findings (Boon et al., 2020; Kumar et al., 2013; Kumar et al., 2016), pSer8-Aβ and pSer26-Aβ showed differential deposition. While pSer8-Aβ deposits primarily in the core of extracellular plaques, pSer26-Aβ showed limited deposition in these lesions (Boon et al., 2020; Kumar et al., 2021). Importantly, pSer8-Aβ was hardly detected within microglia, but mainly deposited as fibrillar Aβ in the plaque core which also contained N-terminally non-modified Aβ. These data are in line with the fibrillization-promoting effect of Aβ phosphorylation at Ser8 (Kumar et al., 2011). Thus, although microglia could bind Ser8-Aβ containing aggregates, their internalization might be restricted by the high compaction of these peptides within the plaque core. In contrast, pSer26-Aβ was prominently detected within plaque-associated microglia. Since the phosphorylation at Ser26 prevents fibrillization but stabilizes oligomeric states of Aβ (Kumar et al., 2016; Rezaei-Ghaleh et al., 2014), soluble pSer26-Aβ assemblies might efficiently bind to TREM2 and be internalized.

Pyroglutamate modified and nitrated Aβ did not show increased binding to TREM2. In contrast to phosphorylation, pyro-glutamination and nitration do not change the overall charge of Aβ. Since TREM2 preferentially binds anionic ligands (Kober & Brett, 2017; Ulrich et al., 2017; Walter, 2016), the additional negative charges introduced by phosphorylation, likely contribute to the increased association of phosphorylated Aβ with TREM2. However, additional effects of distinct post-translational modifications on the conformation and aggregation status of Aβ assemblies could also modulate binding to TREM2. Further, distinct post-translational modifications could affect phagocytosis and degradation pathways of these species as well as their deposition and neurotoxic properties independent on TREM2. Indeed, phosphorylation, nitration, and pyro-glutamination of Aβ differentially affect the aggregation and neurotoxicity of Aβ in in vitro systems without the involvement of TREM2 (Dammers et al., 2015; Kumar et al., 2016; Kummer et al., 2011; Nussbaum et al., 2012). Thus, it will be interesting to further dissect the relative contribution of TREM2 and microglia in the deposition and neurotoxic properties of the different Aβ species in the brain during the pathogenesis of AD.

It should be noted that the deposition of non-modified, pyroglutamate-modified, and phosphorylated Aβ species follows a specific sequence in the brain with initial deposits not containing detectable amounts of pyro-glutaminated or phosphorylated Aβ species (Gerth et al., 2018; Rijal Upadhaya et al., 2014; Thal et al., 2019). While pyro-glutaminated Aβ variants can also be detected in a subset of cases without clinical signs of dementia, detection of phosphorylated Ser8-Aβ is mainly restricted to cases with clinical manifestation of AD (Rijal Upadhaya et al., 2014; Thal et al., 2019). As mentioned above, pSer26-Aβ species show limited deposition in extracellular plaques, but are also found intraneuronally and in vascular deposits (Kumar et al., 2016; Kumar et al., 2021). Thus, post-translational modifications likely contribute to the specific accumulation and differential deposition in the brain and could represent interesting targets for AD therapy.

Indeed, recent data from phase 2 clinical trials revealed positive effects of antibodies specifically recognizing pyroglutamate modified Aβ (Donanemab) in early AD (Mintun et al., 2021). Thus, it will be important to further assess the potential of targeting phosphorylated Aβ species in AD therapy and prevention.

CONFLICT OF INTEREST

The authors declare no competing financial interests.

AUTHOR CONTRIBUTIONS

Pranav Joshi, Paul E. Fraser, Peter St George-Hyslop, and Jochen Walter conceived the study. Pranav Joshi performed most of the experiments and analyzed data. Florian Riffel contributed to cell biological and biochemical interaction studies. Pranav Joshi, Kanayo Satoh, and Masahiro Enomoto performed and analyzed BLI experiments. Seema Qamar purified TREM2 ectodomain for the BLI experiments. Sandra Theil and Sathish Kumar purified modification-specific monoclonal antibodies. Hannah Scheiblich, Nàdia Villacampa, and Michael T. Heneka prepared primary mouse microglia and provided mouse brains. Pranav Joshi and Jochen Walter wrote the manuscript with help from Kanayo Satoh, Paul E. Fraser, and further input from all co-authors. All of the authors read, edited, and approved the final version of the manuscript.

DATA AVAILABILITY STATEMENT

The data of this study is available from the corresponding author upon reasonable request.

ORCID

Pranav Joshi https://orcid.org/0000-0002-1153-0440
Florian Riffel https://orcid.org/0000-0001-8594-100X
Nàdia Villacampa https://orcid.org/0000-0001-6513-0250
Sathish Kumar https://orcid.org/0000-0002-2792-7047
Samira Parhizkar https://orcid.org/0000-0001-5807-190X
Jochen Walter https://orcid.org/0000-0002-4678-2912

REFERENCES

Anderson, V. L., Ramlall, T. F., Rospigliosi, C. C., Webb, W. W., & Eliezer, D. (2010). Identification of a helical intermediate in trifluoroethanol-induced alpha-synuclein aggregation. *Proceedings of the National Academy of Sciences of the United States of America*, 107(44), 18850–18855. https://doi.org/10.1073/pnas.1012336107

Aricescu, A. R., Lu, W., & Jones, E. Y. (2006). A time- and cost-efficient system for high-level protein production in mammalian cells. *Acta Crystallographica. Section D, Biological Crystallography*, 62(Pt 10), 1243–1250. https://doi.org/10.1107/S0907444906029799

Backliwal, G., Hildinger, M., Hasija, V., & Wurm, F. M. (2008). High-density transfection with HEK-293 cells allows doubling of transient titers and removes need for a priori DNA complex formation with PEI. *Biotechnology and Bioengineering*, 99(3), 721–727. https://doi.org/10.1002/bit.21596

Bailey, C. C., DeVaux, L. B., & Farzan, M. (2015). The triggering receptor expressed on myeloid cells 2 binds Apolipoprotein E. *The Journal of Biological Chemistry*, 290(43), 26033–26042. https://doi.org/10.1074/jbc.M115.677286

Barykin, E. P., Mitkevich, V. A., Kozin, S. A., & Makarov, A. A. (2017). Amyloid beta modification: A key to the sporadic Alzheimer's disease? *Frontiers in Genetics*, 8, 58. https://doi.org/10.3389/fgene.2017.00058

Boon, B. D. C., Bulk, M., Jonker, A. J., Morrema, T. H. J., van den Berg, E., Popovic, M., Walter, J., Kumar, S., van der Lee, S. J., Holstege, H., Zhu, X., van Nostrand, W. E., Natté, R., van der Weerd, L., Bouwman, F. H., van de Berg, W. D. J., Rozemuller, A. J. M., & Hoozemans, J. J. M. (2020). The coarse-grained plaque: A divergent Abeta plaque-type in early-onset Alzheimer's disease. *Acta Neuropathologica*, 140(6), 811–830. https://doi.org/10.1007/s00401-020-02198-8

Burgess, R. R. (2009). Protein precipitation techniques. *Methods in Enzymology*, 463, 331–342. https://doi.org/10.1016/s0076-6879(09)63020-2

Condello, C., Yuan, P., Schain, A., & Grutzendler, J. (2015). Microglia constitute a barrier that prevents neurotoxic protofibrillar Abeta42 hotspots around plaques. *Nature Communications*, 6, 6176. https://doi.org/10.1038/ncomms7176

Dammers, C., Gremer, L., Reiß, K., Klein, A. N., Neudecker, P., Hartmann, R., Sun, N., Demuth, H. U., Schwarten, M., & Willbold, D. (2015). Structural analysis and aggregation propensity of Pyroglutamate Abeta(3-40) in aqueous Trifluoroethanol. *PLoS One*, 10(11), e0143647. https://doi.org/10.1371/journal.pone.0143647

d'Errico, P., & Meyer-Luehmann, M. (2020). Mechanisms of pathogenic tau and Abeta protein spreading in Alzheimer's disease. *Frontiers in Aging Neuroscience*, 12, 265. https://doi.org/10.3389/fnagi.2020.00265

Fang, X. T., Sehlin, D., Lannfelt, L., Syvanen, S., & Hultqvist, G. (2017). Efficient and inexpensive transient expression of multispecific multivalent antibodies in Expi293 cells. *Biological Procedures Online*, 19, 11. https://doi.org/10.1186/s12575-017-0060-7

Feuerbach, D., Schindler, P., Barske, C., Joller, S., Beng-Louka, E., Worringer, K. A., Kommineni, S., Kaykas, A., Ho, D. J., Ye, C., Welzenbach, K., Elain, G., Klein, L., Brzak, I., Mir, A. K., Farady, C. J., Aichholz, R., Popp, S., George, N., & Neumann, U. (2017). ADAM17 is the main sheddase for the generation of human triggering receptor expressed in myeloid cells (hTREM2) ectodomain and cleaves TREM2 after Histidine 157. *Neuroscience Letters*, 660, 109–114. https://doi.org/10.1016/j.neulet.2017.09.034

Gerth, J., Kumar, S., Rijal Upadhaya, A., Ghebremedhin, E., von Arnim, C. A. F., Thal, D. R., & Walter, J. (2018). Modified amyloid variants in pathological subgroups of beta-amyloidosis. *Annals of Clinical Translational Neurology*, 5(7), 815–831. https://doi.org/10.1002/acn3.577

Giulian, D., & Baker, T. J. (1986). Characterization of ameboid microglia isolated from developing mammalian brain. *The Journal of Neuroscience*, 6(8), 2163–2178. https://doi.org/10.1523/JNEUROSCI.06-08-02163.1986

Gouras, G. K., Tampellini, D., Takahashi, R. H., & Capetillo-Zarate, E. (2010). Intraneuronal beta-amyloid accumulation and synapse pathology in Alzheimer's disease. *Acta Neuropathologica*, 119(5), 523–541. https://doi.org/10.1007/s00401-010-0679-9

Gouras, G. K., Willen, K., & Tampellini, D. (2012). Critical role of intra-neuronal Abeta in Alzheimer's disease: Technical challenges in studying intracellular Abeta. *Life Sciences*, 91(23–24), 1153–1158. https://doi.org/10.1016/j.lfs.2012.06.004

Guerreiro, R., Bilgic, B., Guven, G., Brás, J., Rohrer, J., Lohmann, E., Hanagasi, H., Gurvit, H., & Emre, M. (2013). Novel compound heterozygous mutation in TREM2 found in a Turkish frontotemporal dementia-like family. *Neurobiology of Aging*, 34(12), 2890.e1–2890.e5. https://doi.org/10.1016/j.neurobiolaging.2013.06.005

Guerreiro, R., Wojtas, A., Bras, J., Carrasquillo, M., Rogaeva, E., Majounie, E., Cruchaga, C., Sassi, C., Kauwe, J. S., Younkin, S., Hazrati, L., Collinge, J., Pocock, J., Lashley, T., Williams, J., Lambert, J. C., Amouyel, P., Goate, A., Rademakers, R., ... Alzheimer Genetic Analysis Group. (2013). TREM2 variants in Alzheimer's disease. *The New England Journal of Medicine*, 368(2), 117–127. https://doi.org/10.1056/NEJMoa1211851

Guerreiro, R. J., Lohmann, E., Brás, J. M., Gibbs, J. R., Rohrer, J. D., Gurunlian, N., Dursun, B., Bilgic, B., Hanagasi, H., Gurvit, H., Emre, M., Singleton, A., & Hardy, J. (2013). Using exome sequencing to reveal mutations in TREM2 presenting as a frontotemporal dementia-like syndrome without bone involvement. *JAMA Neurology*, 70(1), 78–84. https://doi.org/10.1001/jamaneurol.2013.579

Haass, C., & Selkoe, D. J. (2007). Soluble protein oligomers in neurodegeneration: Lessons from the Alzheimer's amyloid beta-peptide. *Nature Reviews. Molecular Cell Biology*, 8(2), 101–112. https://doi.org/10.1038/nrm2101

Hu, Z. W., Ma, M. R., Chen, Y. X., Zhao, Y. F., Qiang, W., & Li, Y. M. (2017). Phosphorylation at Ser(8) as an intrinsic regulatory switch to regulate the morphologies and structures of Alzheimer's 40-residue beta-amyloid (Abeta40) fibrils. *The Journal of Biological Chemistry*, 292(7), 2611–2623. https://doi.org/10.1074/jbc.M116.757179

Huang, Y., Happonen, K. E., Burrola, P. G., O'Connor, C., Hah, N., Huang, L., et al. (2021). Microglia use TAM receptors to detect and engulf amyloid beta plaques. *Nature Immunology*, 22(5), 586–594. https://doi.org/10.1038/s41590-021-00913-5

Hyman, B. T., Phelps, C. H., Beach, T. G., Bigio, E. H., Cairns, N. J., Carrillo, M. C., Dickson, D. W., Duyckaerts, C., Frosch, M. P., Masliah, E., Mirra, S. S., Nelson, P. T., Schneider, J. A., Thal, D. R., Thies, B., Trojanowski, J. Q., Vinters, H. V., & Montine, T. J. (2012). National Institute on Aging-Alzheimer's Association guidelines for the neuropathologic assessment of Alzheimer's disease. *Alzheimers Dement*, 8(1), 1–13. https://doi.org/10.1016/j.jalz.2011.10.007

Ibach, M., Mathews, M., Linnartz-Gerlach, B., Theil, S., Kumar, S., Feederle, R., Brüstle, O., Neumann, H., & Walter, J. (2021). A reporter cell system for the triggering receptor expressed on myeloid cells 2 reveals differential effects of disease-associated variants on receptor signaling and activation by antibodies against the stalk region. *Glia*, 69(5), 1126–1139. https://doi.org/10.1002/glia.23953

Jonsson, T., Stefansson, H., Steinberg, S., Jonsdottir, I., Jonsson, P. V., Snaedal, J., Bjornsson, S., Huttenlocher, J., Levey, A. I., Lah, J. J., Rujescu, D., Hampel, H., Giegling, I., Andreassen, O. A., Engedal, K., Ulstein, I., Djurovic, S., Ibrahim-Verbaas, C., Hofman, A., ... Stefansson, K. (2013). Variant of TREM2 associated with the risk of Alzheimer's disease. *The New England Journal of Medicine*, 368(2), 107–116. https://doi.org/10.1056/NEJMoa1211103

Kim, S. M., Mun, B. R., Lee, S. J., Joh, Y., Lee, H. Y., Ji, K. Y., Choi, H. R., Lee, E. H., Kim, E. M., Jang, J. H., Song, H. W., Mook-Jung, I., Choi, W. S., & Kang, H. S. (2017). TREM2 promotes Abeta phagocytosis by upregulating C/EBPalpha-dependent CD36 expression in microglia. *Scientific Reports*, 7(1), 11118. https://doi.org/10.1038/s41598-017-11634-x

Kim, T., Vidal, G. S., Djurisic, M., William, C. M., Birnbaum, M. E., Garcia, K. C., Hyman, B. T., & Shatz, C. J. (2013). Human LilrB2 is a beta-amyloid receptor and its murine homolog PirB regulates synaptic plasticity in an Alzheimer's model. *Science*, 341(6152), 1399–1404. https://doi.org/10.1126/science.1242077

Kleinberger, G., Yamanishi, Y., Suarez-Calvet, M., Czirr, E., Lohmann, E., Cuyvers, E., Struyfs, H., Pettkus, N., Wenninger-Weinzierl, A.,

Mazaheri, F., Tahirovic, S., Lleo, A., Alcolea, D., Fortea, J., Willem, M., Lammich, S., Molinuevo, J. L., Sanchez-Valle, R., Antonell, A., ... Haass, C. (2014). TREM2 mutations implicated in neurodegeneration impair cell surface transport and phagocytosis. *Science Translational Medicine*, 6(243), 243ra86. https://doi.org/10.1126/scitranslmed.3009093

Kober, D. L., & Brett, T. J. (2017). TREM2-ligand interactions in health and disease. *Journal of Molecular Biology*, 429(11), 1607–1629. https://doi.org/10.1016/j.jmb.2017.04.004

Kober, D. L., Stuchell-Brereton, M. D., Kluender, C. E., Dean, H. B., Strickland, M. R., Steinberg, D. F., Nelson, S. S., Baban, B., Holtzman, D. M., Frieden, C., Alexander-Brett, J., Roberson, E. D., Song, Y., & Brett, T. J. (2020). Functional insights from biophysical study of TREM2 interactions with apoE and Abeta1-42. *Alzheimer's & Dementia*, 17, 475–488. https://doi.org/10.1002/alz.12194

Kumar, S., Kapadia, A., Theil, S., Joshi, P., Riffel, F., Heneka, M. T., & Walter, J. (2021). Novel phosphorylation-state specific antibodies reveal differential deposition of ser26 phosphorylated Aβ species in a mouse model of Alzheimer's disease. *Frontiers in Molecular Neuroscience*, 13, 257. https://doi.org/10.3389/fnmol.2020.619639

Kumar, S., Rezaei-Ghaleh, N., Terwel, D., Thal, D. R., Richard, M., Hoch, M., Mc Donald, J. M., Wüllner, U., Glebov, K., Heneka, M. T., Walsh, D. M., Zweckstetter, M., & Walter, J. (2011). Extracellular phosphorylation of the amyloid beta-peptide promotes formation of toxic aggregates during the pathogenesis of Alzheimer's disease. *The EMBO Journal*, 30(11), 2255–2265. https://doi.org/10.1038/emboj.2011.138

Kumar, S., Singh, S., Hinze, D., Josten, M., Sahl, H. G., Siepmann, M., & Walter, J. (2012). Phosphorylation of amyloid-beta peptide at serine 8 attenuates its clearance via insulin-degrading and angiotensin-converting enzymes. *The Journal of Biological Chemistry*, 287(11), 8641–8651. https://doi.org/10.1074/jbc.M111.279133

Kumar, S., Wirths, O., Stüber, K., Wunderlich, P., Koch, P., Theil, S., Rezaei-Ghaleh, N., Zweckstetter, M., Bayer, T. A., Brüstle, O., Thal, D. R., & Walter, J. (2016). Phosphorylation of the amyloid beta-peptide at Ser26 stabilizes oligomeric assembly and increases neurotoxicity. *Acta Neuropathologica*, 131(4), 525–537. https://doi.org/10.1007/s00401-016-1546-0

Kumar, S., Wirths, O., Theil, S., Gerth, J., Bayer, T. A., & Walter, J. (2013). Early intraneuronal accumulation and increased aggregation of phosphorylated Abeta in a mouse model of Alzheimer's disease. *Acta Neuropathologica*, 125(5), 699–709. https://doi.org/10.1007/s00401-013-1107-8

Kummer, M. P., & Heneka, M. T. (2014). Truncated and modified amyloid-beta species. *Alzheimer's Research & Therapy*, 6(3), 28. https://doi.org/10.1186/alzrt258

Kummer, M. P., Hermes, M., Delekarte, A., Hammerschmidt, T., Kumar, S., Terwel, D., Walter, J., Pape, H. C., König, S., Roeber, S., Jessen, F., Klockgether, T., Korte, M., & Heneka, M. T. (2011). Nitration of tyrosine 10 critically enhances amyloid beta aggregation and plaque formation. *Neuron*, 71(5), 833–844. https://doi.org/10.1016/j.neuron.2011.07.001

le Ber, I., de Septenville, A., Guerreiro, R., Bras, J., Camuzat, A., Caroppo, P., Lattante, S., Couarch, P., Kabashi, E., Bouya-Ahmed, K., Dubois, B., & Brice, A. (2014). Homozygous TREM2 mutation in a family with atypical frontotemporal dementia. *Neurobiology of Aging*, 35(10), 2419.e23–2419. e25. https://doi.org/10.1016/j.neurobiolaging.2014.04.010

Lessard, C. B., Malnik, S. L., Zhou, Y., Ladd, T. B., Cruz, P. E., Ran, Y., Mahan, T. E., Chakrabaty, P., Holtzman, D. M., Ulrich, J. D., Colonna, M., & Golde, T. E. (2018). High-affinity interactions and signal transduction between Abeta oligomers and TREM2. *EMBO Molecular Medicine*, 10(11), e9027. https://doi.org/10.15252/emmm.201809027

Mandrekar, S., Jiang, Q., Lee, C. Y., Koenigsknecht-Talboo, J., Holtzman, D. M., & Landreth, G. E. (2009). Microglia mediate the clearance of soluble Abeta through fluid phase macropinocytosis. *The Journal of Neuroscience*, 29(13), 4252–4262. https://doi.org/10.1523/JNEUROSCI.5572-08.2009

Mintun, M. A., Lo, A. C., Duggan Evans, C., Wessels, A. M., Ardayfio, P. A., Andersen, S. W., Shcherbinin, S., Sparks, J. D., Sims, J. R., Brys, M., Apostolova, L. G., Salloway, S. P., & Skovronsky, D. M. (2021). Donanemab in early Alzheimer's disease. *The New England Journal of Medicine*, 384(18), 1691–1704. https://doi.org/10.1056/NEJMoa2100708

Nussbaum, J. M., Schilling, S., Cynis, H., Silva, A., Swanson, E., Wangsanut, T., Tayler, K., Wiltgen, B., Hatami, A., Rönicke, R., Reymann, K., Hutter-Paier, B., Alexandru, A., Jagla, W., Graubner, S., Glabe, C. G., Demuth, H. U., & Bloom, G. S. (2012). Prion-like behaviour and tau-dependent cytotoxicity of pyroglutamylated amyloid-beta. *Nature*, 485(7400), 651–655. https://doi.org/10.1038/nature11060

Paloneva BM, J., Autti, T., Raininko, R., Partanen, J., Salonen, O., Puranen, M., Hakola, P., & Haltia, M. (2001). CNS manifestations of Nasu-Hakola disease: A frontal dementia with bone cysts. *Neurology*, 56(11), 1552–1558. https://doi.org/10.1212/wnl.56.11.1552

Parhizkar, S., Arzberger, T., Brendel, M., Kleinberger, G., Deussing, M., Focke, C., Nuscher, B., Xiong, M., Ghasemigharagoz, A., Katzmarski, N., Krasemann, S., Lichtenthaler, S. F., Müller, S. A., Colombo, A., Monasor, L. S., Tahirovic, S., Herms, J., Willem, M., Pettkus, N., ... Haass, C. (2019). Loss of TREM2 function increases amyloid seeding but reduces plaque-associated ApoE. *Nature Neuroscience*, 22(2), 191–204. https://doi.org/10.1038/s41593-018-0296-9

Rezaei-Ghaleh, N., Amininasab, M., Giller, K., Kumar, S., Stündl, A., Schneider, A., Becker, S., Walter, J., & Zweckstetter, M. (2014). Turn plasticity distinguishes different modes of amyloid-beta aggregation. *Journal of the American Chemical Society*, 136(13), 4913–4919. https://doi.org/10.1021/ja411707y

Rezaei-Ghaleh, N., Amininasab, M., Kumar, S., Walter, J., & Zweckstetter, M. (2016). Phosphorylation modifies the molecular stability of beta-amyloid deposits. *Nature Communications*, 7, 11359. https://doi.org/10.1038/ncomms11359

Rijal Upadhaya, A., Kosterin, I., Kumar, S., von Arnim, C. A., Yamaguchi, H., Fändrich, M., Walter, J., & Thal, D. R. (2014). Biochemical stages of amyloid-beta peptide aggregation and accumulation in the human brain and their association with symptomatic and pathologically preclinical Alzheimer's disease. *Brain*, 137(Pt 3), 887–903. https://doi.org/10.1093/brain/awt362

Saido, T. C., Iwatsubo, T., Mann, D. M., Shimada, H., Ihara, Y., & Kawashima, S. (1995). Dominant and differential deposition of distinct beta-amyloid peptide species, a beta N3(pE), in senile plaques. *Neuron*, 14(2), 457–466. https://doi.org/10.1016/0896-6273(95)90301-1

Schilling, S., Zeitschel, U., Hoffmann, T., Heiser, U., Francke, M., Kehlen, A., Holzer, M., Hutter-Paier, B., Prokesch, M., Windisch, M., Jagla, W., Schlenzig, D., Lindner, C., Rudolph, T., Reuter, G., Cynis, H., Montag, D., Demuth, H. U., & Rossner, S. (2008). Glutaminyl cyclase inhibition attenuates pyroglutamate Abeta and Alzheimer's disease-like pathology. *Nature Medicine*, 14(10), 1106–1111. https://doi.org/10.1038/nm.1872

Schlepckow, K., Kleinberger, G., Fukumori, A., Feederle, R., Lichtenthaler, S. F., Steiner, H., & Haass, C. (2017). An Alzheimer-associated TREM2 variant occurs at the ADAM cleavage site and affects shedding and phagocytic function. *EMBO Molecular Medicine*, 9(10), 1356–1365. https://doi.org/10.15252/emmm.201707672

Selkoe, D. J., & Hardy, J. (2016). The amyloid hypothesis of Alzheimer's disease at 25 years. *EMBO Molecular Medicine*, 8(6), 595–608. https://doi.org/10.15252/emmm.201606210

Spangenberg, E., Severson, P. L., Hohsfield, L. A., Crapser, J., Zhang, J., Burton, E. A., Zhang, Y., Spevak, W., Lin, J., Phan, N. Y., Habets, G., Rymar, A., Tsang, G., Walters, J., Nespi, M., Singh, P., Broome, S., Ibrahim, P., Zhang, C., ... Green, K. N. (2019). Sustained microglial depletion with CSF1R inhibitor impairs parenchymal plaque development in an Alzheimer's disease model. *Nature Communications*, 10(1), 3758. https://doi.org/10.1038/s41467-019-11674-z

Styren, S. D., Hamilton, R. L., Styren, G. C., & Klunk, W. E. (2000). X-34, a fluorescent derivative of Congo red: A novel histochemical stain for Alzheimer's disease pathology. *The Journal of Histochemistry and Cytochemistry*, 48(9), 1223–1232. https://doi.org/10.1177/002215540004800906

Tamboli, I. Y., Prager, K., Thal, D. R., Thelen, K. M., Dewachter, I., Pietrzik, C. U., St. George-Hyslop, P., Sisodia, S. S., de Strooper, B., Heneka, M. T., Filippov, M. A., Muller, U., van Leuven, F., Lutjohann, D., & Walter, J. (2008). Loss of gamma-secretase function impairs endocytosis of lipoprotein particles and membrane cholesterol homeostasis. *The Journal of Neuroscience*, 28(46), 12097–12106. https://doi.org/10.1523/JNEUROSCI.2635-08.2008

Thal, D. R., Capetillo-Zarate, E., Larionov, S., Staufenbiel, M., Zurbruegg, S., & Beckmann, N. (2009). Capillary cerebral amyloid angiopathy is associated with vessel occlusion and cerebral blood flow disturbances. *Neurobiology of Aging*, 30(12), 1936–1948. https://doi.org/10.1016/j.neurobiolaging.2008.01.017

Thal, D. R., Griffin, W. S., & Braak, H. (2008). Parenchymal and vascular Abeta-deposition and its effects on the degeneration of neurons and cognition in Alzheimer's disease. *Journal of Cellular and Molecular Medicine*, 12(5B), 1848–1862. https://doi.org/10.1111/j.1582-4934.2008.00411.x

Thal, D. R., Ronisz, A., Tousseyn, T., Rijal Upadhaya, A., Balakrishnan, K., Vandenberghe, R., Vandenbulcke, M., von Arnim, C. A. F., Otto, M., Beach, T. G., Lilja, J., Heurling, K., Chakrabarty, A., Ismail, A., Buckley, C., Smith, A. P. L., Kumar, S., Farrar, G., & Walter, J. (2019). Different aspects of Alzheimer's disease-related amyloid beta-peptide pathology and their relationship to amyloid positron emission tomography imaging and dementia. *Acta Neuropathologica Communications*, 7(1), 178. https://doi.org/10.1186/s40478-019-0837-9

Thornton, P., Sevalle, J., Deery, M. J., Fraser, G., Zhou, Y., Ståhl, S., Franssen, E. H., Dodd, R. B., Qamar, S., Gomez Perez-Nievas, B., Nicol, L. S. C., Eketjäll, S., Revell, J., Jones, C., Billinton, A., St George-Hyslop, P. H., Chessell, I., & Crowther, D. C. (2017). TREM2 shedding by cleavage at the H157-S158 bond is accelerated for the Alzheimer's disease-associated H157Y variant. *EMBO Molecular Medicine*, 9(10), 1366–1378. https://doi.org/10.15252/emmm.201707673

Turnbull, I. R., Gilfillan, S., Cella, M., Aoshi, T., Miller, M., Piccio, L., Hernandez, M., & Colonna, M. (2006). Cutting edge: TREM-2 attenuates macrophage activation. *Journal of Immunology*, 177(6), 3520–3524. https://doi.org/10.4049/jimmunol.177.6.3520

Ulrich, J. D., Ulland, T. K., Colonna, M., & Holtzman, D. M. (2017). Elucidating the role of TREM2 in Alzheimer's disease. *Neuron*, 94(2), 237–248. https://doi.org/10.1016/j.neuron.2017.02.042

Verdier, Y., Zarandi, M., & Penke, B. (2004). Amyloid beta-peptide interactions with neuronal and glial cell plasma membrane: Binding sites and implications for Alzheimer's disease. *Journal of Peptide Science*, 10(5), 229–248. https://doi.org/10.1002/psc.573

Vilalta, A., Zhou, Y., Sevalle, J., Griffin, J. K., Satoh, K., Allendorf, D. H., De, S., Puigdellívol, M., Bruzas, A., Burguillos, M. A., Dodd, R. B., Chen, F., Zhang, Y., Flagmeier, P., Needham, L.-M., Enomoto, M., Qamar, S., Henderson, J., Walter, J., ... Brown, G. C. (2021). Wild-type sTREM2 blocks Aβ aggregation and neurotoxicity, but the Alzheimer's R47H mutant increases Aβ aggregation. *Journal of Biological Chemistry*, 296, 100631. https://doi.org/10.1016/j.jbc.2021.100631

Walter, J. (2016). The triggering receptor expressed on myeloid cells 2: A molecular link of Neuroinflammation and neurodegenerative diseases. *The Journal of Biological Chemistry*, 291(9), 4334–4341. https://doi.org/10.1074/jbc.R115.704981

Wang, Y., Cella, M., Mallinson, K., Ulrich, J. D., Young, K. L., Robinette, M. L., Gilfillan, S., Krishnan, G. M., Sudhakar, S., Zinselmeyer, B. H., Holtzman, D. M., Cirrito, J. R., & Colonna, M. (2015). TREM2 lipid sensing sustains the microglial response in an Alzheimer's disease model. *Cell*, 160(6), 1061–1071. https://doi.org/10.1016/j.cell.2015.01.049

Wesen, E., Jeffries, G. D. M., Matson Dzebo, M., & Esbjorner, E. K. (2017). Endocytic uptake of monomeric amyloid-beta peptides is clathrin- and dynamin-independent and results in selective accumulation of Abeta (1-42) compared to Abeta(1-40). *Scientific Reports*, 7(1), 2021. https://doi.org/10.1038/s41598-017-02227-9

Wingfield, P. (2001). Protein precipitation using ammonium sulfate. *Current Protocols in Protein Science*, *Appendix 3*, Appendix 3F. https://doi.org/10.1002/0471140864.psa03fs13

Wirths, O., Breyhan, H., Cynis, H., Schilling, S., Demuth, H. U., & Bayer, T. A. (2009). Intraneuronal pyroglutamate-Abeta 3-42 triggers neurodegeneration and lethal neurological deficits in a transgenic mouse model. *Acta Neuropathologica*, 118(4), 487–496. https://doi.org/10.1007/s00401-009-0557-5

Wunderlich, P., Glebov, K., Kemmerling, N., Tien, N. T., Neumann, H., & Walter, J. (2013). Sequential proteolytic processing of the triggering receptor expressed on myeloid cells-2 (TREM2) protein by ectodomain shedding and gamma-secretase-dependent intramembranous cleavage. *The Journal of Biological Chemistry*, 288(46), 33027–33036. https://doi.org/10.1074/jbc.M113.517540

Xiang, X., Werner, G., Bohrmann, B., Liesz, A., Mazaheri, F., Capell, A., Feederle, R., Knuesel, I., Kleinberger, G., & Haass, C. (2016). TREM2 deficiency reduces the efficacy of immunotherapeutic amyloid clearance. *EMBO Molecular Medicine*, 8(9), 992–1004. https://doi.org/10.15252/emmm.201606370

Yeh, F. L., Wang, Y., Tom, I., Gonzalez, L. C., & Sheng, M. (2016). TREM2 binds to Apolipoproteins, including APOE and CLU/APOJ, and thereby facilitates uptake of amyloid-Beta by microglia. *Neuron*, 91(2), 328–340. https://doi.org/10.1016/j.neuron.2016.06.015

Yu, Y., & Ye, R. D. (2015). Microglial Abeta receptors in Alzheimer's disease. *Cellular and Molecular Neurobiology*, 35(1), 71–83. https://doi.org/10.1007/s10571-014-0101-6

Yuan, P., Condello, C., Keene, C. D., Wang, Y., Bird, T. D., Paul, S. M., Luo, W., Colonna, M., Baddeley, D., & Grutzendler, J. (2016). TREM2 Haplodeficiency in mice and humans impairs the microglia barrier function leading to decreased amyloid compaction and severe axonal dystrophy. *Neuron*, 90(4), 724–739. https://doi.org/10.1016/j.neuron.2016.05.003

Zhao, Y., Wu, X., Li, X., Jiang, L.-L., Gui, X., Liu, Y., Sun, Y., Zhu, B., Piña-Crespo, J. C., Zhang, M., Zhang, N., Chen, X., Bu, G., An, Z., Huang, T. Y., & Xu, H. (2018). TREM2 is a receptor for β-amyloid that mediates microglial function. *Neuron*, 97(5), 1023–1031.e7. https://doi.org/10.1016/j.neuron.2018.01.031

Zhong, L., Wang, Z., Wang, D., Wang, Z., Martens, Y. A., Wu, L., Xu, Y., Wang, K., Li, J., Huang, R., Can, D., Xu, H., Bu, G., & Chen, X. F. (2018). Amyloid-beta modulates microglial responses by binding to the triggering receptor expressed on myeloid cells 2 (TREM2). *Molecular Neurodegeneration*, 13(1), 15. https://doi.org/10.1186/s13024-018-0247-7

SUPPORTING INFORMATION

Additional supporting information may be found in the online version of the article at the publisher's website.